Polymer 49 (2008) 4647–4651

Contents lists available at ScienceDirect

Polymer

journal homepage: www.elsevier.com/locate/polymer

Synthesis of MDMO-PPV capped PbS quantum dots and their application to solar cells

Zhijie Wang [a], Shengchun Qu [a,*], Xiangbo Zeng [a], Changsha Zhang [a], Mingji Shi [a], Furui Tan [a], Zhanguo Wang [a], Junpeng Liu [b], Yanbing Hou [c], Feng Teng [c], Zhihui Feng [c]

[a] Key Laboratory of Semiconductor Materials Science, Institute of Semiconductors, Chinese Academy of Sciences, P. O. Box 912, Beijing 100083, PR China
[b] College of Chemistry and Molecular Engineering, Peking University, Beijing 100871, PR China
[c] Key Laboratory of Luminescence and Optical Information, Ministry of Education, Institute of Optoelectronic Technology, Beijing Jiaotong University, Beijing 100044, PR China

ARTICLE INFO

Article history:
Received 19 May 2008
Received in revised form 21 August 2008
Accepted 28 August 2008
Available online 3 September 2008

Keywords:
Hybrid solar cells
Polymer
PbS quantum dots

ABSTRACT

Poly[2-methoxy-5-(3′,7′-dimethyloctyloxy)-1,4-phenylenevinylene] (MDMO-PPV) capped PbS quantum dots about 3–6 nm in diameter were synthesized with a novel method. Unlike the synthesis of oleic acid capped PbS quantum dots, the reactions were carried out in solution at room temperature, with the presence of a capping ligand species, MDMO-PPV. The quantum dots were used to fabricate bulk heterojunction solar cells with an indium tin oxide (ITO)/polyethylenedioxythiophene/polystyrenesulphonate (PEDOT: PSS)/MDMO-PPV: PbS/Al structure. Current density–voltage characterization of the devices showed that after the addition of the MDMO-PPV capped PbS quantum dots to MDMO-PPV film, the performance was dramatically improved compared with pristine MDMO-PPV solar cells.

1. Introduction

The increasing demand for energy has already forced us to seek more environmentally clean energy resources. Solar radiation is ideal to meet the demand on energy. At the present time, the solar cells based on semiconductors such as Si and GaAs remain limited due to the high costs imposed by fabrication procedures involving elevated temperature, high vacuum, and numerous lithographic steps [1]. Due to the potential increase in energy conversion efficiency of quantum dot (QD) solar cells to about 66% [2] and the low fabrication cost, hybrid organic/inorganic QD bulk heterojunction (BHJ) solar cells fabricated by a solution process have attracted considerable attentions. Beek et al. [3,4] used nanocrystal ZnO as an *n*-type semiconductor to blend with MDMO-PPV as the active layer of BHJ solar cells, and the overall energy conversion efficiency reached 1.6%. The cost is reduced but the efficiency is low for the low charge mobility and low absorption in the near infrared (NIR) spectrum. Sun et al. [5] reported the solar cells based on the blends of CdSe tetrapods and poly(*p*-phenylenvinylene) derivative OC_1C_{10}-PPV, and the maximum energy conversion efficiency reached 2.8%. This enhanced performance over ZnO hybrid solar cells is due to both the absorption and the charge transport improvement resulting from CdSe's narrow bandgap and tetrapods morphology in nanometer scale. However, CdSe is toxic and can damage the environment and the human body.

With a narrow bandgap of 0.41 eV, a large exciton Bohr radius (18 nm) and a strong quantum-size effect in nanocrystalline form, PbS is widely used in many fields such as solar cells [6–11], infrared detectors [6,12], infrared electroluminescent devices [13,14], and optical switches [15]. Furthermore, an efficient multiple exciton generation has been detected in PbS QD, thus rendering it a promising candidate for highly efficient photovoltaic devices [16,17]. There are many routes to prepare PbS QDs with different surfactants [18–24]. The most successful QDs used in solar cells and photodetectors are oleic acid capped PbS QDs or their post-synthetic ligand exchange products [8,25,26]. However, the 2.5-nm-long oleic acid ligand inhibits charge transport among the nanocrystals. To improve charge transport, a post-synthetic ligand exchange is used to replace the oleic acid with shorter ligands. However, this adds complexity to the process. Furthermore, the shorter ligands still impede charge transport between QDs or different materials.

Using a polymer as surfactant of the nanocrystals can overcome the disadvantage of the insulator surfactants, and the hybrid materials show different morphologies [27] and applications. Poly(*N*-isopropylacrylamide) (PNIPAM) has been used as the surfactant in fabrication gold nanoparticles by reduction of $HAuCl_4$ in aqueous solution [28]. Chausson et al. [29] reported that a nanostructured organic/inorganic hybrid material can be synthesized via an acido-basic reaction and the modification of the

* Corresponding author. Fax: +86 010 82305052.
E-mail address: qsc@semi.ac.cn (S. Qu).

0032-3861/$ – see front matter © 2008 Elsevier Ltd. All rights reserved.
doi:10.1016/j.polymer.2008.08.041

titanoniobate oxide $KTiNbO_5$ by *N*-alkyl amines. The silica based hybrid materials have also attracted lots of attentions [30–33] as well as phosphate glass/polymer hybrids [34] due to some unique properties. In this paper, we propose a method to prepare PbS QDs directly in MDMO-PPV solution. High-resolution transmission electron microscopy (HRTEM) images show that the MDMO-PPV capped PbS QDs have a narrow size distribution with diameters in the range of 3–6 nm. Blending MDMO-PPV with MDMO-PPV capped PbS QDs as the active layer, BHJ solar cells were fabricated. The current density–voltage (*J–V*) measurement shows that the devices with an active layer of MDMO-PPV hybrid with the PbS QDs are better in photovoltaic performance than those with the polymer only.

2. Experimental

2.1. Synthesis of MDMO-PPV capped PbS quantum dots

A total of 10 mg MDMO-PPV (purchased from Aldrich) was dissolved in 30 mL toluene to form an orange semi-transparent solution. After 10 min of stirring, 6 mL dimethylsulfoxide (DMSO) was added and the solution became transparent immediately. Then 100 mg lead acetate ($Pb(OAc)_2$) was added. Once the $Pb(OAc)_2$ was dissolved in the solution completely, 3 mL DMSO solution containing 12 mg thioacetamide (TAA) was added dropwise under vigorous stirring. After 20 min, the color of the solution changed from orange to dark red, and the solution retained some transparency. The resulting dark red solution was precipitated by adding excess ethanol. The precipitate was centrifuged at 7000 rpm for 6 min to remove the unwanted molecular byproducts and washed with ethanol several times. The weight of the final product was about 20 mg, indicating that the PbS was about 10 mg after subtracting the weight of MDMO-PPV.

2.2. Fabrication of the BHJ solar cells

The photovoltaic devices were fabricated by spin-coating a blend of the capped PbS QDs and MDMO-PPV in an appropriate ratio, sandwiched between a transparent anode and a cathode. The anode consisted of ITO pre-coated glass substrate modified by a spin-coating PEDOT: PSS layer. The cathode was aluminum. Before device fabrication, the ITO-coated glass substrate was cleaned by detergent, deionized water, acetone and isopropyl alcohol sequentially, in an ultrasonic bath. A thin layer of PEDOT: PSS (Baytron 4083) was spin-coated to modify the ITO surface and annealed at 140 °C for 10 min. Then the substrate was transferred to a nitrogen-filled glove box. MDMO-PPV was first dissolved in chlorobenzene to make a 6 mg/mL solution, followed by blending it with the PbS QDs. The blend was ultrasonicated for 1 h and stirred for 3 h, and then transferred to the nitrogen-filled glove box. The active layer was obtained by spin-coating the blend at 1500 rpm for 30 s. After the active layer was annealed in the glove box at 110 °C for 22 h, aluminum was deposited under a high vacuum as the cathode. As a reference, pristine polymer solar cell structured as ITO/PEDOT: PSS/MDMO-PPV/Al was fabricated, and the solar cells with different annealing processes were also produced. Fig. 1 shows the structure of the solar cells.

2.3. Characterization

HRTEM for MDMO-PPV capped PbS QDs was performed using a TECNAI F20 TEM equipped with a field emission gun operating at 200 kV accelerating voltage. Ultraviolet–visible–near infrared (UV–vis–NIR) absorption spectrum was carried out by an UV-3100 UV–vis–NIR recording spectrophotometer (Shimadzu). Photoluminescence (PL) spectrum was carried out at room temperature

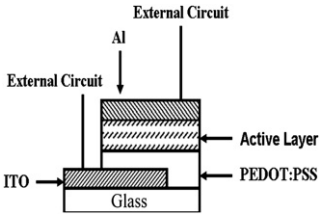

Fig. 1. Structure of the solar cells.

(Edinburgh Instruments Ltd., FLS 920). *J–V* measurements were performed in forward bias with a computer-controlled Keithley 2400 Source Meter under ~100 mW/cm^2 illumination from a solar simulator. A 500 W xenon lamp served as the light source and the light intensity was calibrated using a standard silicon solar cell. In the *J–V* measurement process, the fill factor (FF) was calculated using

$$\mathrm{FF} = (J \times V)_{\max}/(J_{\mathrm{sc}} \times V_{\mathrm{oc}}) \quad (1)$$

where $(J \times V)_{\max}$ is the maximum product of *J* and *V* that can be calculated from the *J–V* curve, J_{sc} is the short circuit current density and the V_{oc} is the open circuit voltage. Defined as the ratio of the electric power output of the cell at the maximum power point to the incident optical power (P_{light}), the energy conversion efficiency (EFF) can be calculated using the following equation.

$$\mathrm{EFF} = \mathrm{FF} \times J_{\mathrm{sc}} \times V_{\mathrm{oc}}/P_{\mathrm{light}} \quad (2)$$

Series resistance (R_{ss}) and shunt resistance (R_{sh}) were obtained from the *J–V* curve directly by using

$$R_{\mathrm{ss}} = (\mathrm{d}V/\mathrm{d}I)I = 0 \quad (3)$$

and

$$R_{\mathrm{sh}} = (\mathrm{d}V/\mathrm{d}I)_{V=0} \quad (4)$$

respectively.

3. Results and discussions

3.1. Characterization of MDMO-PPV capped PbS quantum dots

MDMO-PPV cannot dissolve in DMSO but can in toluene, while $Pb(OAc)_2$ cannot dissolve in toluene but can in DMSO. So, we blended the two solutions in an appropriate ratio to dissolve the two reactants. When TAA solution was added dropwise under vigorous stirring, MDMO-PPV capped PbS was formed, accompanied by the change in the color from orange to dark red. The resultant can be dispersed in toluene and chlorobenzene homogeneously. To confirm the existence of PbS, energy dispersive spectroscopy (EDS) was measured. Fig. 2 demonstrates that the main elements of the sample are Pb and S. The peaks of C, Cu, and O are from the copper grid substrate.

TEM and HRTEM, shown in Fig. 3, were used to examine the PbS growth and quality. From the images, PbS QDs, somehow aggregating, are found. The aggregation may result for the following reasons. First, for smaller QDs, there exists a weak, albeit long-range attraction that persists up to higher concentrations in the solution of polymer and QDs [35]. Second, for small QDs, the absorption of polymer on the surface of QDs mainly happens in the form of tails [35], and when the solution vaporizes, the tails may link the QDs together. Through the measurement of EDS, the dark particles are PbS QDs. The grey areas without crystal lattice between them may be the MDMO-PPV. The sizes of QDs are from 3 to 6 nm in diameter, marked by the arrow in Fig. 3a. Fig. 3b is the

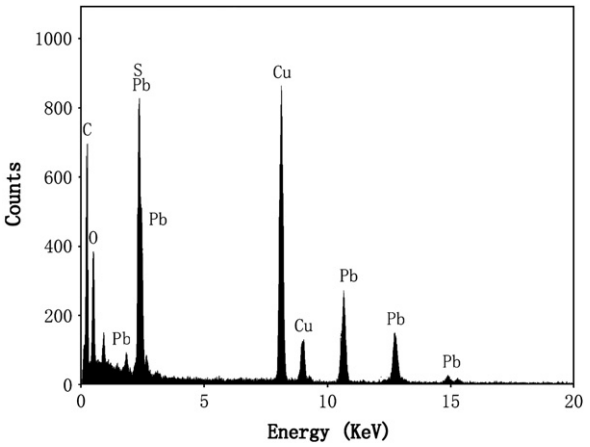

Fig. 2. EDS spectrum of the MDMO-PPV capped PbS QDs.

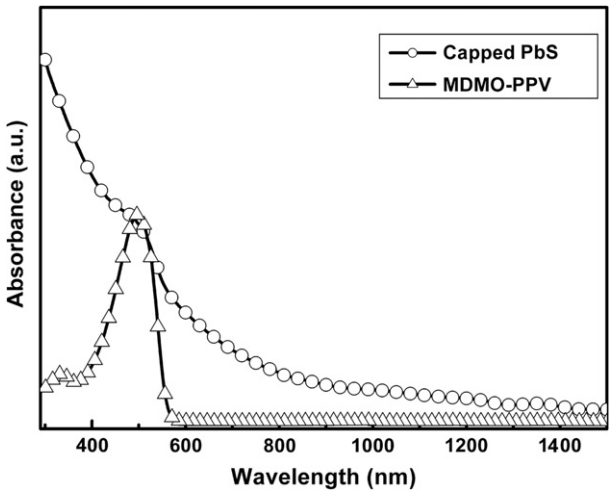

Fig. 4. UV–vis–NIR absorption spectra of the MDMO-PPV capped PbS QDs (excess MDMO-PPV was removed) and pristine MDMO-PPV. The measurement was made from solution with a 0.1 mg/mL concentration. The absorption spectra were normalized at the absorption peak of the MDMO-PPV (500 nm).

HRTEM image of the dark particles in Fig. 3a, which clearly demonstrates the lattice structure for the QDs.

In order to reduce the influence of the MDMO-PPV in the measurement of absorption spectrum, the final product containing 50 wt% MDMO-PPV and 50 wt% PbS QDs was dissolved in toluene and centrifuged at 10,000 rpm to remove the excess MDMO-PPV that was not absorbed on the QD surface. Bulk PbS has an absorption peak at 3020 nm corresponding to a small bandgap of 0.41 eV at 298 K [26], and the peak in PbS nanocrystallite should significantly blue-shift as a consequence of strong quantum confinement. Fig. 4 demonstrates the UV–vis–NIR absorption spectrum of the PbS QDs, which extends significantly in both the NIR and UV ranges as compared with that of the pristine MOMD-PPV, further confirming the existence of PbS in the MDMO-PPV matrix. At about 500 nm, there is a shoulder in the absorption spectrum of the MDMO-PPV capped PbS QDs. The shoulder results from the absorption of the MDMO-PPV on the surface of the QDs. Beyond 600 nm where MDMO-PPV has no absorption, the absorption is mainly from the PbS QDs. Beyond 1500 nm, there is no absorption at all. This blue-shift absorption as compared with bulk PbS confirms that the MDMO-PPV capped PbS has a nanometer size smaller than the Bohr radius.

The distance of Forster transfer of energy is 5–10 nm [36], and the distance of Dexter transfer of energy is 0.5–1 nm [37], and both the energy transfer routes can be facilitated due to the direct contact of MDMO-PPV with the PbS QDs. Furthermore, the charge transfer between the two materials is also facilitated. Fig. 5 shows the PL spectra of MDMO-PPV and MDMO-PPV capped PbS QDs under 466 nm illumination from a xenon lamp. Compared with MDMO-PPV, the MDMO-PPV capped PbS QDs show a significantly lower PL intensity at the peak of MDMO-PPV, which suggests the PL quenching of the MDMO-PPV by the PbS QDs in the composite. As the weight of the capped PbS QDs decreases to 25 wt% in proportion,

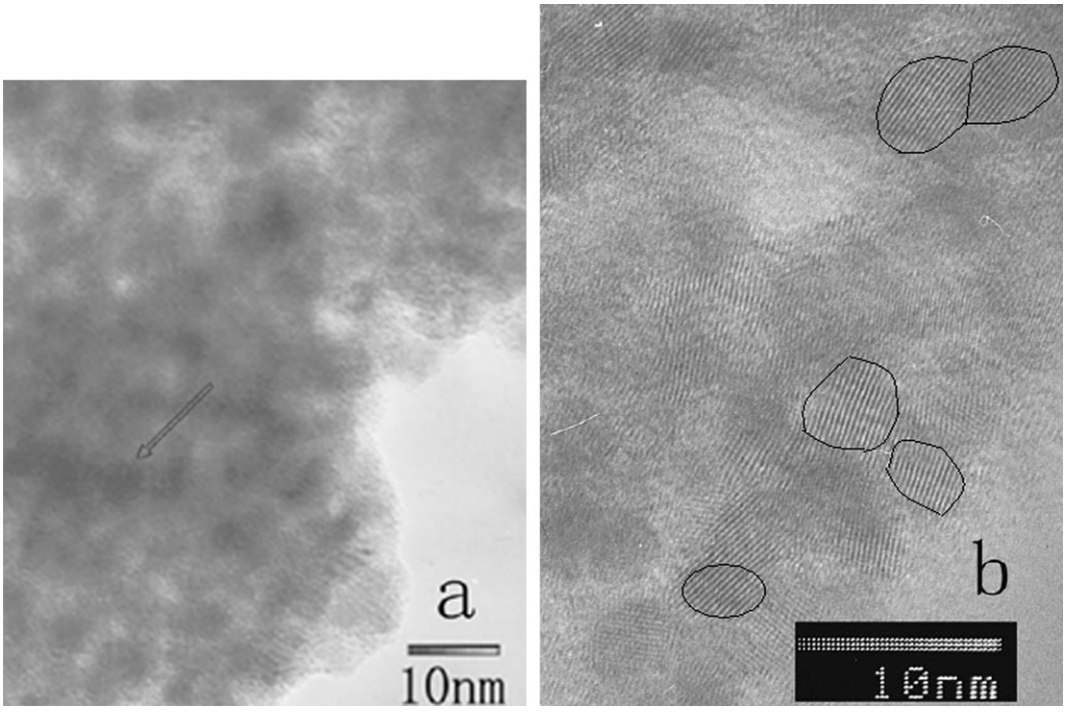

Fig. 3. TEM and HRTEM images of the MDMO-PPV capped PbS QDs.

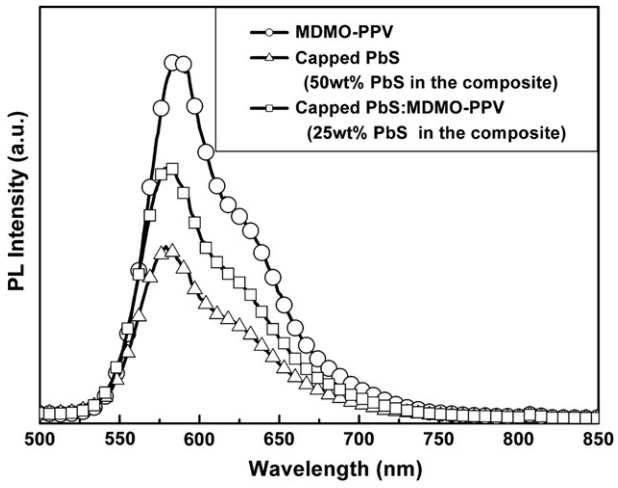

Fig. 5. PL spectra of MDMO-PPV, MDMO-PPV capped PbS QDs (50 wt% PbS) and MDMO-PPV: MDMO-PPV capped PbS QDs (25 wt% PbS), under illumination of 466 nm from a xenon lamp. The spectra were measured from the thin films spin-coated with the same solution dosage of 0.5 mL and MDMO-PPV concentration of 3 mg/mL at 1500 rpm on the quartz substrate.

the PL intensity of MDMO-PPV increases. This quenching process is usually accompanied by the charge transfer between the two materials, the electron generated by the dissociation of an exciton in the polymer transfers to the PbS QDs, while the hole remains in the polymer. The charge and energy transfer processes are crucial for the efficiency improvement of BHJ solar cells.

3.2. Performance of solar cells

UV–vis–NIR absorption spectroscopy was recorded to investigate the effect on absorption of adding MDMO-PPV capped PbS QDs to the MDMO-PPV solution used for spin-coating the active layer. In order to capture the true solar cells absorption change when capped PbS QDs were added to the MDMO-PPV thin film, samples were prepared directly on the PEDOT: PSS modified ITO glass. The absorption spectrum of the active layer should be equal to the difference between the transmission spectrum of the bilayer structure of ITO/PEDOT: PSS and that of triple-layer structure of ITO/PEDOT: PSS/active layer, with reflection being neglected. Fig. 6 shows the UV–vis–NIR absorption spectra of the pristine MDMO-PPV, MDMO-PPV capped PbS QDs and MDMO-PPV: MDMO-PPV capped PbS QDs (1:2 in weight) thin films on the PEDOT: PSS modified ITO glass. Unlike the absorption spectrum of MDMO-PPV on the quartz substrate, the absorption spectrum of MOMD-PPV on PEDOT: PSS modified ITO glass is relatively wide and low in intensity in the NIR range, which may result from the influence of PEDOT: PSS modified ITO glass. Not only the intensity but also the range of the absorption spectrum is improved by adding PbS QDs to the pristine MDMO-PPV thin film. Compared with the pure MDMO-PPV capped PbS QDs thin film, the MDMO-PPV: MDMO-PPV capped PbS QDs thin film is lower in absorption intensity below 800 nm, due to the decrease of PbS QDs concentration. The improved absorption, which enhances the exciton generation efficiency, is one of the most important factors in improving the efficiency of solar cells.

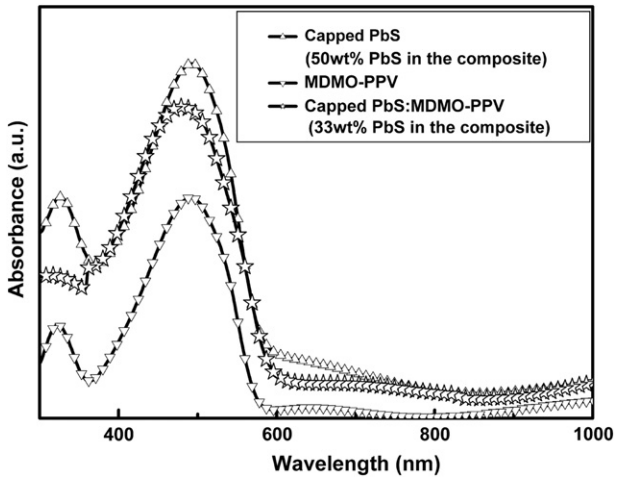

Fig. 6. UV–vis–NIR absorption spectra of MDMO-PPV capped PbS QDs (50 wt% PbS), pristine MDMO-PPV and MDMO-PPV: MDMO-PPV capped PbS QDs (33 wt% PbS) thin films spin-coated with the same solution dosage (0.5 mL) and MDMO-PPV concentration (6 mg/mL) at 1500 rpm on PEDOT: PSS coated ITO glass.

However, there are also some important factors that affect the energy conversion efficiency, such as exciton diffusion, exciton dissociation, charge transport and charge collection. All of these have a relationship with the film structure and morphology. Fig. 7 shows the *J–V* curves of solar cells with different active layers. Compared with the solar cell with pristine MDMO-PPV as the active layer, the solar cell with MDMO-PPV blended with MDMO-PPV capped PbS QDs as the active layer has an energy conversion efficiency 16 times larger than that of the pristine solar cell. The improvement of the energy conversion efficiency results from the increase of open circuit voltage (V_{OC}), short circuit current density (J_{SC}), FF, R_{sh}, and the reduction of R_{ss}.

For the pristine MDMO-PPV solar cells, once the radiation enters the active layer, it can be absorbed by photoexcitation of the polymer, followed by the generation of an exciton. The exciton can diffuse, recombine, or dissociate in the active layer. The diffusion length of the excitons in polymer is usually smaller than 10 nm, so when the excitons travel longer than 10 nm, most of them decay. This process is the main loss process in polymer based solar cells. Because of the high exciton binding energy in conjugated polymers, the thermal energy at room temperature is not sufficient to dissociate a photogenerated exciton with the typical binding energy of 0.4 eV into free charge carriers, so the exciton cannot dissociate into free charge carriers in the polymer itself. Due to the difference in work function, only the excitons generated near electrodes dissociate into free charge carriers. This is the most important reason for the low energy conversion efficiency in pristine polymer solar cells.

The conditions change in the BHJ solar cells. Once the radiation enters the active layer, it can be absorbed by photoexcitation both of the polymer and PbS QDs, followed by the generation of excitons. Thus, the generation efficiency is higher than that in pristine solar cells. Because of the direct blending of MDMO-PPV with MDMO-PPV capped PbS QDs, the travel length of the excitons can be

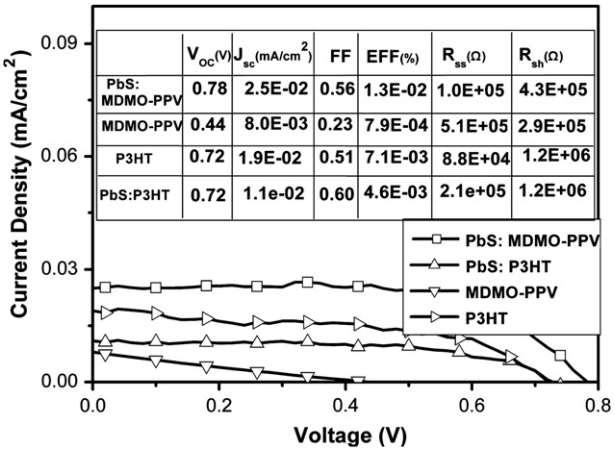

	V_{OC}(V)	J_{sc}(mA/cm^2)	FF	EFF(%)	R_{ss}(Ω)	R_{sh}(Ω)
PbS: MDMO-PPV	0.78	2.5E-02	0.56	1.3E-02	1.0E+05	4.3E+05
MDMO-PPV	0.44	8.0E-03	0.23	7.9E-04	5.1E+05	2.9E+05
P3HT	0.72	1.9E-02	0.51	7.1E-03	8.8E+04	1.2E+06
PbS:P3HT	0.72	1.1e-02	0.60	4.6E-03	2.1e+05	1.2E+06

Fig. 7. *J–V* curves of the BHJ solar cells with different active layer structures.

reduced below the diffusion length through the careful control on morphology. Most of the excitons can travel to the interface of the polymer and PbS QDs. In the role of the difference of the highest occupied molecular orbital (HOMO) of MDMO-PPV and the lowest unoccupied molecular orbital (LUMO) of the PbS QDs, the excitons can dissociate into free charge carriers that contribute to the current of the solar cells. The electrons transport in the PbS QDs and are collected by the Al electrode, while the holes transport along the polymer and are collected by the ITO electrode. From our PL measurement, profound PL quenching was achieved when the capped PbS QDs were added to MDMO-PPV film, which confirms that most of the excitons dissociate into free charge carriers and the excitons' dissociation efficiency is improved. When the holes and the electrons transport in the polymer and PbS QDs, respectively, the recombination of the charge carriers is reduced, which appears as the decrease of R_{ss} and increase of R_{sh}.

Furthermore, we also produced poly(3-hexylthiophene) (P3HT) capped PbS QDs and used them to fabricate BHJ solar cells. Surprisingly, it is found that the P3HT capped PbS QDs: P3HT BHJ solar cells are worse in performance than the pristine polymer solar cells. The V_{oc} and the R_{sh} are nearly the same, while J_{sc} is reduced and R_{ss} is increased. This can be explained by the decreased hole transport in P3HT when PbS QDs are added into the P3HT film, though the exciton generation and dissociation efficiency are improved.

Annealing is an effective way to control the film morphology, especially at temperatures above the glass transition temperature (T_g) of the polymer. Annealing near or above T_g allows morphology changes in the film that might yield more favorable electrical transport properties in both the polymer and nanocrystal phases. Such morphology changes could thus yield a more efficient BHJ structure in the film, and improve both charge separation and transport. Fig. 8 shows the *J–V* curves of the BHJ solar cells with different annealing processes. Although the samples without an annealing process (shown as the "nonan" samples in Fig. 8) show higher V_{oc}, the annealed solar cells show even higher J_{sc} and FF. Thus, the energy conversion efficiency of the annealed samples is improved dramatically. This improvement of J_{sc} FF and R_{ss} of the annealed solar cells indicates the improvement of charge separation and transport. After the active layer was annealed at 110 °C for 22 h, the Al electrode was deposited, and then the samples were annealed at 110 °C for 16 h again. These samples are shown as "prepost" samples in Fig. 6. Compared with the solar cells that were only annealed before Al electrode deposition and are shown as "pre" in Fig. 6, these samples show a worse performance in V_{oc}, J_{sc}, FF, R_{sh} and R_{ss} as well as a significantly reduced energy conversion efficiency. This may result from the diffusion of Al atoms to the active layer during the annealing process, which may inhibit charge separation and transport.

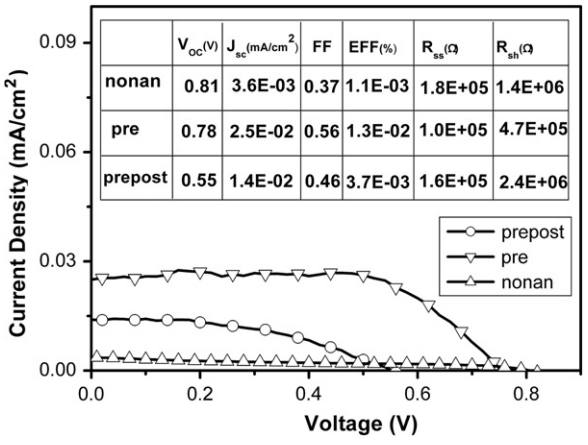

Fig. 8. *J–V* curves of the BHJ solar cells with different annealing processes.

4. Conclusion

MDMO-PPV capped PbS QDs were prepared and used as acceptor in the active layer of BHJ solar cells. The absorption spectra showed that adding the QDs to the polymer can not only improve the absorption in the polymer region but also the beyond that region in both the NIR and UV ranges. This is an important factor in improving the solar cell efficiency. To optimize the performance of the solar cells, the influence of the active layer structure and the effect of thermal annealing were studied. The BHJ solar cell with the highest energy conversion efficiency in this experiment is that with the structure of ITO/PEDOT: PSS/MDMO-PPV: MDMO-PPV capped PbS QDs/Al annealed at 110 °C for 22 h in N_2 before aluminum deposition. The energy conversion efficiency is about 0.013%, more than one order in magnitude higher than that of the pristine polymer solar cell.

Acknowledgments

This work is supported by the National Natural Science Foundation of China (Contract Nos. 60736034, 60576036) and the National Basic Research Program of China with Contract Nos. 2006CB202604 and 2006CB604904, the National High Technology Research and Development Program of China with Contract Nos. 2006AA03Z408.

References

[1] Huynh WU, Dittmer JJ, Alivisatos AP. Science 2002;295:2425–7.
[2] Nozik AJ. Physica E 2002;14:115–20.
[3] Beek WJE, Wienk MM, Janssen RAJ. Adv Mater 2004;16(12):1009–13.
[4] Beek WJE, Wienk MM, Kemerink M, Yang X, Janssen RAJ. J Phys Chem B 2005;109:9505–16.
[5] Sun B, Snaith HJ, Dhoot AS, Westenhoff S, Greenham NC. J Appl Phys 2005;97(1):014914–6.
[6] Mcdonald SA, Konstantatos G, Zhang S, Cyr PW, Klem EJD, Levina L, et al. Nat Mater 2005;4:138–42.
[7] Zhang S, Cyr PW, Mcdonald SA, Konstantatos G, Sargent EH. Appl Phys Lett 2005;87:233101-1–3.
[8] Günes S, Fritz KP, Neugebauer H, Sariciftci NS, Kumar S, Scholes GD. Sol Energy Mater Sol Cells 2007;91:420–3.
[9] Wang P, Wang L, Ma B, Li B, Qiu Y. J Phys Chem B 2006;110:14406–9.
[10] Bayon R, Musembi R, Belaidi A, Bär M, Guminskaya T, Lux-Steiner M -Ch, et al. Sol Energy Mater Sol Cells 2005;89:13–25.
[11] Klem EJD, MacNeil DD, Cyr PW, Levina L, Sargent EH. Appl Phys Lett 2007;90(18):183113-1–3.
[12] Gadenne P, Yagil Y, Deutscher G. J Appl Phys 1989;66(7):3019–25.
[13] Kanstantatos G, Huang C, Levina L, Lu Z, Sargent EH. Adv Funct Mater 2005;15:1865–9.
[14] Hines MA, Scholes GG. Adv Mater 2003;15(21):1844–9.
[15] Kane RS, Cohen RE, Silbey R. J Phys Chem 1996;100:7928–32.
[16] Schaller RD, Sykora M, Pietryga JM, Klimov VI. Nano Lett 2006;6:424–9.
[17] Ellingson RJ, Beard MC, Johnson JC, Yu P, Micic OI, Nozik AJ, et al. Nano Lett 2005;5(5):865–71.
[18] Qu F, Silva RS, Dantas NO. Phys Stat Sol B 2002;232(1):95–9.
[19] Lu X, Zhao Y, Wang C. Adv Mater 2005;17:2485–8.
[20] Choudhury KR, Sahoo Y, Jang S, Prasad PN. Adv Funct Mater 2005;15(5):751–6.
[21] Watt A, Thomsen E, Meredith P, Dunlop HR. Chem Commun 2004:2334–5.
[22] Zhou Y, Itoh H, Uemura T, Naka K, Chujo Y. Langmuir 2002;18:5287–92.
[23] Wu S, Zeng H, Schelly ZA. Langmuir 2005;21:686–91.
[24] Zhang Z, Lee SH, Vittal JJ, Chin WS. J Phys Chem B 2006;110:6649–54.
[25] Konstantatos G, Howard I, Fischer A, Hoogland S, Clifford J, Klem E, et al. Nature 2006;422:180–3.
[26] Hawaldar RR, Kanadeb KG, Patilc KR, Sathayed SD, Mulika UP, Amalnerkar DP. Mater Chem Phys 2005;91:447–53.
[27] Pietsch T, Gindy N, Fahmi A. Polymer 2008;49:914–21.
[28] Aqil A, Qiu H, Greisch J, Jérôme R, Pauw ED, Jérôme C. Polymer 2008;49:1145–53.
[29] Chausson S, Caignaert V, Retoux R, Rueff J, Pluart LL, Madec P, et al. Polymer 2008;49:488–96.
[30] Guo Q, Thomann R, Gronski W. Polymer 2007;48:3925–9.
[31] Li S, Shah A, Hsieh AJ, Haghighat R, Praveen SS, Mukherjee I, et al. Polymer 2007;48:3982–9.
[32] Chang C, Tzeng H. Polymer 2006;47:8536–47.
[33] Ogoshi T, Chujo Y. Polymer 2006;47:4036–41.
[34] Urman K, Madbouly S, Otaigbe JU. Polymer 2007;48:1659–66.
[35] Surve M, Pryamitsyn V, Ganesan V. Langmuir 2006;22:969–81.
[36] Berlman IB. New York: Academic Press; 1973.
[37] Dexter DL. J Chem Phys 1953;21:836–50.